Dominant magnetic-dipole nuclear excitation by electron capture in a beam-based scenario for the ^{84m}Rb isomer

K. Słabkowska,[1,*] Ł. Syrocki,[2] M. Polasik,[1] J. J. Carroll,[3] C. J. Chiara,[3] and J. Rzadkiewicz[4]

[1]*Faculty of Chemistry, Nicolaus Copernicus University in Toruń, Gagarina 7, 87-100 Toruń, Poland*

[2]*Institute of Plasma Physics and Laser Microfusion, Hery 23, 01-497 Warsaw, Poland*

[3]*U.S. Army Combat Capabilities Development Command Army Research Laboratory, Adelphi, Maryland 20783, USA*

[4]*National Centre for Nuclear Research, 05-400 Otwock, Poland*

(Received 8 March 2024; accepted 26 April 2024; published 29 May 2024)

Here, we consider nuclear excitation by electron capture (NEEC) in a beam-based experiment for the ^{84m}Rb isomer ($I^{\pi} = 6^{-}$, $T_{1/2} = 20.26$ min). The NEEC process for the ^{84m}Rb isomer allows an excitation by magnetic-dipole ($M1$) and electric-quadrupole ($E2$) transitions into a depletion level ($I^{\pi} = 5^{-}$), which subsequently decays, releasing a substantial amount of stored energy. To ensure effective production of the ^{84m}Rb isomer, the fusion-evaporation reaction ^{82}Se + ^{7}Li is considered. In the multiconfigurational Dirac-Fock calculations of energy released by electron capture into the M, N, O, P, and Q shells, we have used the ground-state configurations for ^{84m}Rb ions. To focus on the role of $M1$ and $E2$ transition multipolarities, Compton profiles, and excited-state configurations are neglected here. The predictions of the mean equilibrium charge state for the ^{84m}Rb recoil ion as a function of its kinetic energy in the C target and the analysis of potentially possible NEEC resonance kinetic energies have been performed. The NEEC resonance strengths and probabilities have been estimated by a theoretical model applied for the $M1$ and $E2$ excitations. It was found that the $M1$ contribution for the NEEC process clearly dominates over the $E2$ one. Moreover, the total NEEC probability ($M1$ plus $E2$) for ^{84m}Rb isomer is almost three orders of magnitude higher than that predicted for the ^{93m}Mo isomer. This result makes the ^{84m}Rb isomer a good candidate for new NEEC beam-based experiment.

DOI: 10.1103/PhysRevC.109.054327

I. INTRODUCTION

A limited number of isotopes occur in nuclear isomeric states (i.e., metastable excited states of atomic nuclei) which are characterized by long-sometimes extremely long-lifetimes in the range from nanoseconds to many years (e.g., the lifetime for the ^{180m}Ta isomer is at least 10^{17} y, much longer than the age of the Universe) [1,2]. Some of these long-lived isomers can store a huge amount of energy, up to a few MeV per nucleus [3], and have been proposed for extremely high-density energy storage materials (nuclear batteries). Therefore, considerable research has been conducted to investigate a means by which to induce the release of stored energy on demand [3].

One of the possible mechanisms for inducing this energy release is the isomer depletion via the nuclear excitation by electron capture (NEEC) process [4–7]. In the NEEC process, an electron is captured into an unfilled atomic subshell of an isomer-containing ion with the simultaneous excitation of the nucleus to a higher-energy state. NEEC can occur when the initial (precapture) kinetic energy of the electron plus the electron binding energy released upon its capture matches the energy difference between the two nuclear states.

For capture of a free electron, this mechanism, as originally conceived in 1976 by Goldanskii and Namiot, is the inverse of the internal conversion (IC) process discovered about 100 years ago and was correspondingly dubbed inverse internal electron conversion (IIEC) [4]. Only excitations from the nuclear ground state were treated in Ref. [4]. In 1989, Cue, Poizat, and Remillieux considered a similar scenario, but with the excitation of the nucleus of a projectile ion arising from capture of a *target-bound* electron; they coined the term NEEC [8] which, in later theoretical developments, e.g., Refs. [6,7], supplanted the name IIEC for free-electron capture as well. Zadernovsky and Carroll later extended the NEEC concept to excitations from a nuclear isomer, rather than the ground state, as a mechanism for isomer depletion [5]. Very recently Carroll and Chiara published a review article on isomer depletion [9].

For many decades there were unsuccessful attempts to observe the NEEC process, e.g., with ^{242}Am in an electron beam ion trap (EBIT) [10] and with bare ^{57}Fe ions channeling in a Si crystal [11]. In 2007, Pálffy *et al.* [7] presented the resonance strengths for NEEC processes for the isomers of a few nuclides. In 2006 and 2008, Pálffy *et al.* considered NEEC in storage-ring scenarios [6,12]. In more recent years, Gunst *et al.*, Wu *et al.*, and Wang *et al.* performed theoretical studies of NEEC in laser-generated and EBIT plasmas [13–17]. Additionally, Borisyuk *et al.* and Dzyublik investigated the NEEC process preceded by the laser photoionization [18–20].

*katarzyna.slabkowska@uni.torun.pl

In 2012, Karamian and Carroll published an article [21] in which they suggested conducting an experiment concerning the depletion of the ^{93m}Mo isomer through the NEEC process using a helium gas target in a beam-based scenario. In 2017 we performed an extensive study on the optimal conditions for the first experimental evidence of the NEEC process for the long-lived 6.85-h ^{93m}Mo [22] isomer using the beam-based scenario proposed in Ref. [21]. Our results have supported the first observation [23] of isomer depletion via the NEEC process for the ^{93m}Mo isomer, i.e., the identification of a new physical phenomenon, using the Digital Gammasphere [24] γ-ray spectrometer installed at the linear accelerator facility (ATLAS) at Argonne National Laboratory. The confirmation for the evidence of the ^{93m}Mo isomer depletion via the NEEC process was the unique registration, in coincidence, of the characteristic γ-ray sequence 2475 keV-268 keV-685 keV-1478 keV. The depletion probability obtained in the experiment was unexpectedly high, $P_{\mathrm{NEEC}} = 0.010(3)$ per ^{93m}Mo ion [23].

The theoretical investigation performed by Wu *et al.* [25], attempting to model the ATLAS experiment concerning ^{93m}Mo isomer depletion via the NEEC process, led to predicted NEEC excitation probabilities that are nine orders of magnitude smaller [25] than the experimental results [23]. Therefore, further experimental and theoretical research on ^{93m}Mo [26,27] and other nuclides is desirable to understand the origin of this discrepancy. In other theoretical analyses [28,29], we identified optimal beam-based scenario experimental conditions both for the creation of the ^{242m}Am and ^{110m}Ag isomeric states as well as for the NEEC process in light solid targets.

In 2021, Guo *et al.* suggested a possible overestimation of the ^{93m}Mo isomer depletion probability due to residual contamination arising from chance coincidences [30]. In the response to this, it was shown that the experimental result is largely supported by the suitable background subtraction and extensive analysis techniques [31]. In 2022, Guo *et al.* attempted to experimentally observe the NEEC process for the ^{93m}Mo isomer at the Heavy Ion Research Facility in Lanzhou [32]. In that experiment, the ^{93m}Mo isomer depletion was not observed, and an upper limit of 2×10^{-5} was reported for the NEEC probability [32]. It deserves mention, however, that the ^{93m}Mo recoil energies were substantially lower in Ref. [32] than in Ref. [23] and thus inadequately duplicated the experiment of Ref. [23]. The configuration of implantation materials used in Ref. [23] was also not reproduced in Ref. [32].

Recently, we proposed for the ^{93m}Mo isomer an advanced approach [33] for the theoretical description of the NEEC process that accounts for the effect of bound target electrons on the resonant transfer process (NEEC-RT). Although our paper [33] transforms the quasidiscrete model of the NEEC process into a hitherto unexplored continuous model as a function of the projectile energy in beam-based conditions, the obtained NEEC probability results for the ^{93m}Mo isomer explain only a part of the huge discrepancy between the theory of Ref. [25] and experiment. In addition, we added to a state-of-the-art NEEC-RT model the excited electron configurations for ^{93m}Mo ions [34], moving the theoretical limit farther toward the reported experimental value [23].

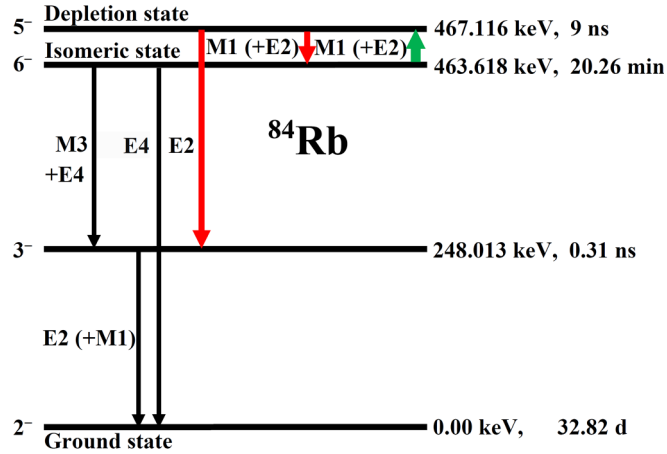

FIG. 1. Partial level scheme (not to scale) for ^{84}Rb. The green arrow describes the transition excited by the NEEC process and the black arrows show the natural decay cascade from the isomer. The red arrows present nuclear transitions following the NEEC process. The multipolarities and $T_{1/2}$ are taken from [35], and the nuclear level energies deduced from [36].

In this paper we consider another beam-based experiment related to the ^{84m}Rb isomer ($T_{1/2} = 20.26$ min). For this isomer, the NEEC process can occur by the magnetic dipole $M1$ and electric quadrupole $E2$ nuclear excitations from the isomeric state (IS, $I^{\pi} = 6^-$) to a depletion state (DS, $I^{\pi} = 5^-$), which lies only a few keV higher in energy. In 2017, Denis-Petit *et al.* deduced a new value $\Delta E = 3.498$ keV for the $5^- \rightarrow 6^-$ transition energy in ^{84}Rb [36]. We adopted this latter value for all our theoretical considerations. We consequently adopted the energy values of the $3^- \rightarrow 2^-$ (248.013 keV), $6^- \rightarrow 2^-$ (463.618 keV), and $5^- \rightarrow 3^-$ (219.099 keV) nuclear transitions measured in Ref. [36]. The DS is, itself, a shorter-lived (9 ns) isomer that subsequently decays through a cascade of transitions to the ground state, releasing a substantial amount of stored energy, as illustrated in Fig. 1. The ^{84}Rb depletion state decays to a 3^- state through a 219.099-keV $E2$ transition that offers a good opportunity for identification of the NEEC process. It should be mentioned here that the depletion of the ^{84m}Rb isomer in the field of the x-ray laser was also considered. It was found that using a free electron laser facility with a peak power of $S_0 = 6 \times 10^{15}$ W/cm^2, the depletion probability for the ^{84m}Rb (6^-) isomer can reach 2×10^{-7} [37]. In this paper, the NEEC resonance strengths and NEEC probabilities have been estimated for the ^{84m}Rb isomer by applying the theoretical model to both the $M1$ and $E2$ nuclear excitations. The role of Compton profiles and excited-state configurations are neglected herein to focus on the role of the multipolarity of the excitation transition from isomer to DS.

Figure 2 shows a general scheme for the beam-based ^{84m}Rb isomer production and its depletion via NEEC. The scheme is based on the idea of separating (in space and time) three processes: production of ^{84}Rb nuclei, feeding of the ^{84m}Rb isomeric state from excited recoiling ^{84}Rb* ions, and finally providing optimal conditions for NEEC to occur. The high-energy recoil ^{84}Rb ions produced in inverse-kinematics fusion-evaporation reactions will move at high speed in the

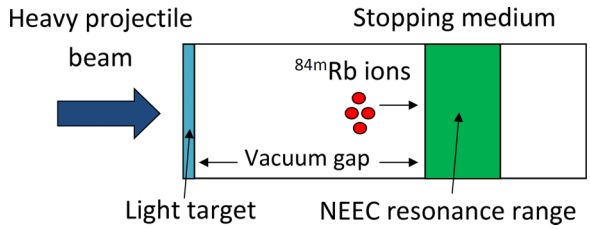

FIG. 2. General scheme for experimental observation of ^{84m}Rb isomer depletion via the NEEC process. Not to scale.

vacuum gap (where the feeding of the ^{84m}Rb isomer occurs; the size of the gap must accommodate the cumulative lifetime of the feeding of the isomer) and then the ^{84m}Rb isomer starts penetrating the stopping medium. Since the lifetimes of the high-spin states produced in the ^{84}Rb nucleus in the fusion evaporation reaction are similar to those in the case of ^{93}Mo, the vacuum gap between the 'production' target and the 'NEEC' target should be of the order of 3 mm (as was the case with the experiment with ^{93m}Mo [23]). During the slowing down process, highly ionized ^{84m}Rb isomeric ions can reach the appropriate energy and atomic state to match, at some point along their paths, the NEEC resonance conditions. A suitable detector system would be needed to observe the ^{84m}Rb isomer production and the subsequent signals confirming that NEEC has occurred. In particular, the detection system dedicated for the beam-based experiment should distinguish the 219.099-keV $E2$ decay of the DS from the 215.605-keV $M3 + E4$ decay of the IS. This can be done either by appropriate coincidence conditions or by energy separation with high-resolution detectors.

II. NUCLEAR-REACTION PRODUCTION OF ^{84}Rb NUCLEI

The cross sections for ^{84}Rb production in the ^{82}Se + ^{7}Li fusion-evaporation reaction have been predicted using the Projection Angular-momentum Coupled Evaporation (PACE4) [38,39] and GEMINI + + [40–42] packages. The PACE4 package is a fusion-evaporation code based on a Monte Carlo statistical-model approach [43]. The PACE4 code enables the user to calculate the cross sections for the compound nucleus (CN) formation and its decay into residual nuclei and other light particles like neutrons, protons, and α particles. The input nucleus-nucleus fusion cross sections are obtained from the Bass model [44], while the transmission coefficients for light particle emission are obtained using the optical-model potential [45]. The calculations account for the recoil energy of the CN and angular distributions of the residual nucleus and light particles.

The GEMINI + + code also employs a Monte Carlo technique to simulate the decay chains of the CN by modes of sequential binary decays until further decay becomes energetically forbidden or very unlikely due to the dominance of γ-ray emission. The CN is assumed in the model to be formed only in a complete fusion reaction with the excitation energy derived from a Q value. Because fusion reactions typically lead to the formation of a CN with large intrinsic angular momenta, the GEMINI + + model takes into account the influence of spin and orbital angular momentum on particle emission. The code employs the sharp-cutoff spin distribution for the CN with a maximum spin value and a cutoff parameter according to Ref. [41]. The model includes all possible decay channels from light-particle emission to symmetric division. The evaporation of neutrons, protons, and other light particles is treated with the Hauser-Feshbach formalism [46], that assumes a distribution of Coulomb barriers arising from large thermal fluctuations. The origin of this distribution may be a result of CN deformation, its density, or its surface diffuseness. More details concerning the PACE4 and GEMINI + + codes can be found in [38–42].

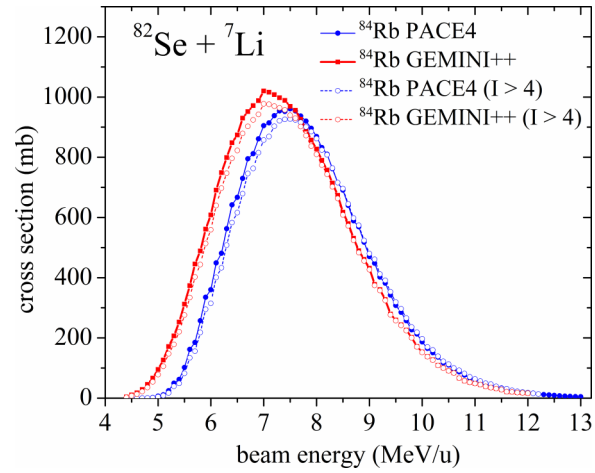

FIG. 3. Cross sections for the production of ^{84}Rb isotopes with desirable ^{84m}Rb isomers (with spins $I > 4$) in the ^{82}Se + ^{7}Li reaction as a function of the beam energy, calculated with the GEMINI + + and PACE4 codes.

Figure 3 presents the cross sections predicted for the ^{82}Se + ^{7}Li reaction leading to the production of ^{84}Rb. As can be seen in the figure, both theoretical predictions obtained using the PACE4 and GEMINI + + codes give very similar shapes of the cross-section function. The cross sections for the ^{84}Rb isotope production range from 4.3 MeV/u to 13 MeV/u, reaching a maximum ($\approx$ 1000 mb) for energies of 7.1–7.4 MeV/u for both codes. Based on these data, one can expect a very effective production of ^{84}Rb isotopes with the desirable ^{84m}Rb isomers ($I > 4$). This production can be up to two orders of magnitude higher than that obtained with reactions ^{7}Li(^{90}Zr, $p3n$) and ^{12}C(^{86}Kr, $5n$) used to produce the ^{93m}Mo isomers in the Argonne and Lanzhou NEEC experiments, respectively [23,32].

III. NEEC ATOMIC-RESONANCE CONDITIONS FOR ^{84m}Rb ISOMERS IN A BEAM-BASED SCENARIO

The kinetic energies required for the NEEC process to occur have been predicted for the M, N, O, P, and Q shells of ^{84m}Rb ions and combined with available ion charge states at subsequent stages of the ion stopping process. The mean equilibrium charge states (q_{mean}) of the ^{84m}Rb ions as a function of the kinetic energy were predicted by means of the Schiwietz and Grande formulas [47]. Figure 4 presents

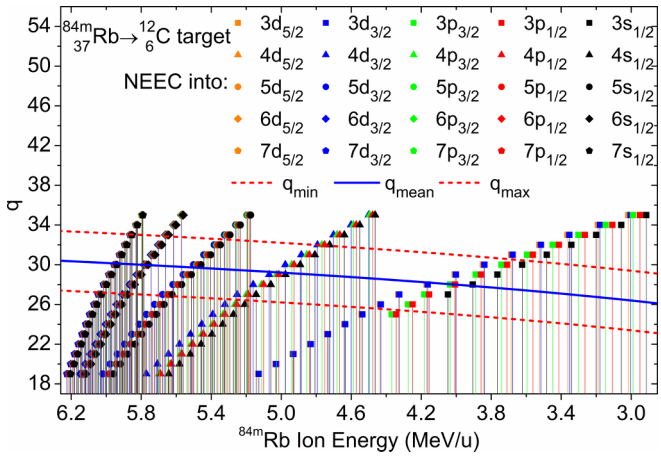

FIG. 4. The q_{mean} of the ^{84m}Rb projectile as a function of its kinetic energy for a ^{12}C stopping target (blue solid line). The top of the vertical bars presents the potential positions of the ^{84m}Rb ion NEEC resonance kinetic energy for shells with $n = 3$ (squares), $n = 4$ (triangles), $n = 5$ (circles), $n = 6$ (diamonds), and $n = 7$ (pentagons) which can occur for the charge states (vertical axis), from $q = +19$ to $q = +35$, indicated by the symbols at the tops of the bars.

this dependence for a ^{12}C stopping target. As can be seen, the q_{mean} of the ^{84m}Rb ions is in the region between $q = +25$ and $q = +30$. The uncertainties of the q_{mean}, obtained from Ref. [47] as a deviation of the experimental values ($\Delta q = \pm 3.0$) from the fit curve for a C solid target, are also shown by two dashed red lines.

The relativistic multiconfigurational Dirac-Fock (MCDF) method, which takes into account the Breit and quantum electrodynamics corrections [48–51], has been used to obtain the values of resonance kinetic energies required for the NEEC process to occur in the case of electron capture into specific atomic subshells for assumed configurations. The MCDF calculations included the appropriate atomic energy levels in ^{84m}Rb ions with the main quantum number $3 \leqslant n \leqslant 7$ and the orbital quantum number $0 \leqslant l \leqslant 2$. In the MCDF calculations of energy released by electron capture into the M, N, O, P, and Q shells, we have used the ground-state configurations for ^{84}Rb ions with the charge states from $q = +19$ to $q = +35$. The potential NEEC resonance kinetic energy of the free electron (in the ^{84m}Rb ion reference frame) has been obtained as a difference between the energy required for NEEC to occur (3.498 keV) and the energy released by electron capture. To obtain the corresponding NEEC resonance kinetic energy of the ^{84m}Rb ion (presented in Fig. 4), we have multiplied the above data by the nucleon-to-electron mass ratio.

Figure 4 presents all potentially possible values of the ^{84m}Rb isomer kinetic energies required for the NEEC process to occur. The most appropriate kinetic energy values for the NEEC process may be seen when the bar tops of the subshells, marked with symbols, reach the area between the two dashed red lines, describing the q_{mean} deviation values of the ^{84m}Rb ion. For each discrete charge state q studied for the given shells ($n = 3$ to 7), each group of five bars illustrates, from right to left, electron capture into the $s_{1/2}$, $p_{1/2}$, $p_{3/2}$, $d_{3/2}$, and $d_{5/2}$ subshells.

One can see that the most appropriate NEEC-process resonance conditions for electron capture into $n = 3$ subshells of ^{84m}Rb ions can be achieved for charge states from $q = +26$ up to $q = +30$ at kinetic energies in a wide range 3.6–4.4 MeV/u. The optimal NEEC process resonance conditions for $n = 4$ subshells can be fulfilled for kinetic energies ranging from about 4.7 up to 5.3 MeV/u for ^{84m}Rb ions with $+26 \leqslant q \leqslant +32$, while for $n = 5$ subshells in a range 5.3−5.7 MeV/u with $+27 \leqslant q \leqslant +32$. In the case of $n = 6$ and $n = 7$ subshells of ^{84m}Rb ions, the most optimal NEEC-process resonance conditions are for charge states $+27 \leqslant q \leqslant +33$ at kinetic energies range 5.7–5.9 MeV/u and 5.9–6.1 MeV/u, respectively. The above data indicate that the NEEC process can occur for relatively low kinetic energies of projectiles, which is very beneficial from the experimental point of view. The NEEC process in ^{84m}Rb can occur for orbitals with a wide range of n (in particular for high n orbitals).

IV. $M1$ AND $E2$ TRANSITIONS FOR NEEC RESONANCE STRENGTHS AND PROBABILITIES

To estimate the NEEC resonance strength for ^{84m}Rb isomers in the proposed above beam-based scenario with low-Z stopping media, we have applied the approach originally presented in Ref. [52] in which the electron-nuclear interaction is attempted to be described with an accurate treatment. In this approach the NEEC cross section for the specific charge state q, subshell nl_j at the incident electron energy E is given by

$$\sigma^{q,nl_j}_{\text{NEEC}}(E) = g\frac{\pi}{2k^2}\frac{\Gamma^{q,nl_j}_N \Gamma^q_r}{(E - E_r)^2 + \frac{1}{4}\left(\Gamma^q_r\right)^2}, \tag{1}$$

where k is the wave number of the incident electron, Γ^{q,nl_j}_N is the width of the nuclear transition from the IS to the DS, and E_r is the resonance energy. The natural resonance width Γ^q_r is the sum of the electronic and nuclear widths. The factor g is a function of the nuclear spins and the total angular momentum of the captured electron. To obtain the resonance strength of the NEEC process for a given atomic state, one has to integrate the cross section over the relative energy of the captured electron

$$S^{q,nl_j}_{\text{NEEC}} = \int \sigma^{q,nl_j}_{\text{NEEC}}(E)dE. \tag{2}$$

Finally, the resonance strengths of the $M1$ and $E2$ NEEC process for the ^{84m}Rb isomer take a modified form of the expression presented in Refs. [28,33]:

$$S^{q,nl_j}_{\text{NEEC}}(\text{M1}) = g\frac{\lambda_e^2}{4}\frac{\alpha^{q,nl_j}_{IC}(\text{M1:DS} \to 6^-)\Gamma_\gamma(\text{M1:DS} \to 6^-)}{\Gamma_{\text{tot}}(\text{DS})} \times \left(1 + \alpha^{q=0}_{IC}(\text{E2:DS} \to 3^-)\right) \times \Gamma_\gamma(\text{E2:DS} \to 3^-), \tag{3}$$

$$S^{q,nl_j}_{\text{NEEC}}(\text{E2}) = g\frac{\lambda_e^2}{4}\frac{\alpha^{q,nl_j}_{IC}(\text{E2:DS} \to 6^-)\Gamma_\gamma(\text{E2:DS} \to 6^-)}{\Gamma_{\text{tot}}(\text{DS})} \times \left(1 + \alpha^{q=0}_{IC}(\text{E2:DS} \to 3^-)\right) \times \Gamma_\gamma(\text{E2:DS} \to 3^-). \tag{4}$$

TABLE I. The NEEC resonance strengths for the $M1$ and $E2$ transitions from the ^{84m}Rb isomer for capture into nl_j subshells with binding energies (E_b) and kinetic energies (E_c) for ions with charge states q.

q	Type	nl_j	E_b (eV)	E_c (MeV/u)	$S^{q,nl_j}_{\rm NEEC}$ (b eV)
+27	$M1$	$3s_{1/2}$	1293.9	4.05	7.6×10^{-3}
+27	$M1$	$3p_{1/2}$	1235.1	4.16	1.0×10^{-3}
+27	$M1$	$3p_{3/2}$	1220.4	4.18	7.1×10^{-4}
+30	$M1$	$4s_{1/2}$	834.1	4.89	4.7×10^{-3}
+33	$M1$	$5s_{1/2}$	615.7	5.29	3.5×10^{-3}
+27	$E2$	$3s_{1/2}$	1293.9	4.05	1.7×10^{-8}
+27	$E2$	$3p_{1/2}$	1235.1	4.16	1.3×10^{-6}
+27	$E2$	$3p_{3/2}$	1220.4	4.18	4.8×10^{-6}
+30	$E2$	$4p_{3/2}$	807.9	4.94	2.7×10^{-6}
+33	$E2$	$5p_{3/2}$	604.3	5.31	1.9×10^{-6}

The parameter λ_e is the wavelength of the electrons prior to capture with the relative resonance energy E_r. The $\Gamma_\gamma(M1\text{: DS} \to 6^-)$, $\Gamma_\gamma(E2\text{: DS} \to 6^-)$, and $\Gamma_\gamma(E2\text{: DS} \to 3^-)$ are the $M1$ and $E2$ radiative transition widths and $\Gamma_{\rm tot}$(DS) is the total width of the DS ($I^\pi = 5^-$). As the reduced transition probabilities for the $M1$: DS $\to 6^-$ and $E2$: DS $\to 6^-$ nuclear transitions we employed values from nuclear shell-model calculations: $B(M1: 5^- \to 6^-) = 0.116$ W.u. and $B(E2: 5^- \to 6^-) = 0.762$ W.u. [36,53,54]. The reduced transition probability for the $E2$: DS $\to 3^-$ nuclear transition was taken from [35]. The $\alpha_{IC}^{q=0}$ ($E2$: DS $\to 3^-$) is the total internal conversion coefficient (ICC) for the $E2$: DS $\to 3^-$ transition for a neutral ^{84m}Rb atom, where the ICC is defined as the ratio of the electron to gamma emission rates. This total ICC was calculated as a sum of contributions from all sub-shells ($1s_{1/2}$, $2s_{1/2}$, $2p_{1/2}$, etc.) of a neutral atom (^{84m}Rb$^{q=0}$) with the frozen orbital approximation based on Dirac-Fock calculations. It was shown that the ICC predictions based on the Dirac-Fock calculations can reproduce the experimental values at about 1% levels of accuracy [55,56]. The α_{IC}^{q,nl_j} ($M1$: DS $\to 6^-$) and α_{IC}^{q,nl_j} ($E2$: DS $\to 6^-$) ICCs for ^{84m}Rb^q ions were estimated by applying a scaling procedure that relates the ICCs to the binding energies and the number of available vacancies for the specific q ($+19 \leqslant q \leqslant +35$) in a given subshell (from $3s_{1/2}$ up to $7d_{5/2}$) [28,33,57].

In Table I, we present the NEEC resonance strengths for $M1$ and $E2$ transitions from the ^{84m}Rb isomer following electron capture into selected nl_j subshells for $n \geqslant 3$ (NEEC for the K and L shells is energetically forbidden for ^{84m}Rb) and for several charge states q. As one can see, the $M1$ NEEC resonance strengths are several orders of magnitude higher than those for $E2$ NEEC. Among the $M1$ NEEC resonance strengths, the most dominant contribution is for the $3s_{1/2}$ subshell. Moreover, $M1$ NEEC into the $4s_{1/2}$ and $5s_{1/2}$ subshells is also much more intense than those into the $3p_{1/2}$ and $3p_{3/2}$ subshells. For $E2$ NEEC, the highest contribution is from the $3p_{3/2}$ subshell; however, contributions from other analyzed subshells are also non-negligible.

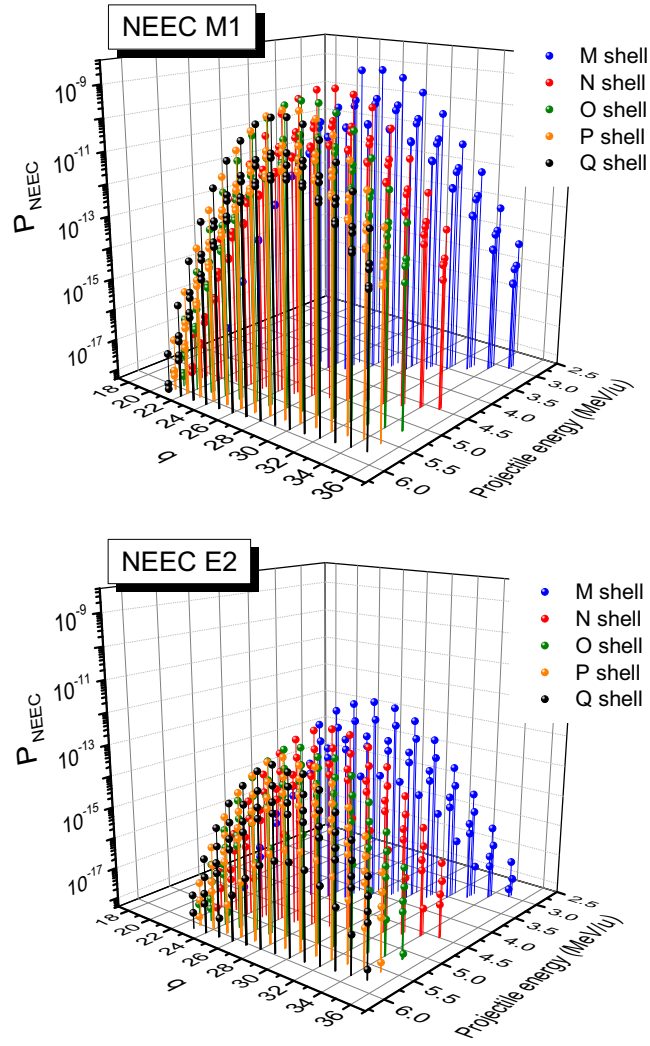

FIG. 5. NEEC partial probabilities $P_{\rm NEEC}$ for electron captures into M, N, O, P, and Q shells as a function of the projectile energy and charge state q of ^{84m}Rb ions in the case of $M1$ and $E2$ transitions.

The total NEEC probability can be determined as a sum of partial NEEC contributions for capture into nl_j subshells and for ion charge states [25]

$$P_{\rm NEEC} = \frac{m_p}{m_e} n_e \sum_{q,nl_j} \frac{f_q\left(E_p^{q,nl_j}\right) S^{q,nl_j}_{\rm NEEC}\left(E_p^{q,nl_j}\right)}{-(dE/dx)|_{E_p^{q,nl_j}}}, \qquad (5)$$

where dE/dx is the stopping power, f_q is the charge-state fraction, n_e is the electron density, and m_p and m_e are the masses of the projectile and electron, respectively. In Fig. 5 we present the NEEC partial probabilities $P_{\rm NEEC}$ for electron captures into the M, N, O, P, and Q shells as a function of the projectile energy and charge state q for $M1$ and $E2$ transitions from ^{84m}Rb. As one can see, the partial probabilities obtained for $M1$ transitions are about three orders of magnitude higher than those obtained for $E2$ transitions. The highest probabilities for the NEEC process for the $M1$ transitions are for electron capture into the M shell for a charge state q in the range of $+25 \leqslant q \leqslant +30$ and low projectile energy from 3.7

TABLE II. Total and partial (for L, M, N, O, P, and Q shells) $M1$ and $E2$ NEEC probabilities for ^{84m}Rb and ^{93m}Mo isomers.

Isomer	Type	L shell	M shell	N shell	O shell	P shell	Q shell	Total
^{84m}Rb	$M1$	-	7.12×10^{-9}	5.52×10^{-9}	3.78×10^{-9}	2.78×10^{-9}	2.13×10^{-9}	2.13×10^{-8}
^{84m}Rb	$E2$	-	6.21×10^{-12}	3.52×10^{-12}	2.07×10^{-12}	1.51×10^{-12}	1.17×10^{-12}	1.45×10^{-11}
^{93m}Mo[a]	$E2$	5.68×10^{-18}	1.53×10^{-11}	7.54×10^{-12}	3.77×10^{-12}	-	-	2.66×10^{-11}

[a]Wuet al. [25].

to 4.4 MeV/u. For capture into the N shell, slightly lower probabilities for $+19 \leqslant q \leqslant +35$ and projectile energy from 4.5 to 5.8 MeV/u are the result of lower $M1$ NEEC resonance strengths. Moreover, in general the probabilities for the Q shell are the smallest, but still significant for $+19 \leqslant q \leqslant +35$ and projectile energy from 5.8 to 6.2 MeV/u. The situation is similar in the case of the NEEC process for the $E2$ transitions. The highest probabilities are for electron capture into the M shell, then one can see a gradual decrease in the probabilities for the higher shells down to the lowest probabilities occurring for the Q shell.

In addition, our theoretical predictions for the total and partial (for M, N, O, P, and Q shells) probabilities of the NEEC process for the ^{84m}Rb isomer are presented in Table II. Previous theoretical predictions for the ^{93m}Mo isomer [25] are also shown. As can be seen for the ^{84m}Rb isomer, the total and partial (for all shells) NEEC probabilities we obtained for the $M1$ NEEC are almost three orders of magnitude higher than those obtained for the $E2$ NEEC. Among the $M1$ NEEC probabilities, the most dominant contribution is for the M shell with slightly smaller contributions for higher shells up to the smallest but still significant contribution for the electron capture into the Q shell. One can also expect that subsequent shells would have a noticeable contribution to the total NEEC probability.

In the case of the $E2$ NEEC process, in addition to the clearly visible much lower total and partial probabilities compared to the $M1$ NEEC process, at a close look one can also see that the $E2$ NEEC partial probabilities show a stronger reduction for increasingly higher atomic shells than the corresponding partial probabilities for the $M1$ NEEC. This is the result of the dominance of two different orbital types for the $M1$ and $E2$ NEEC processes, respectively. In the case of $M1$ NEEC, the highest resonance strengths and probabilities occur for electron capture into the $ns_{1/2}$ orbitals, for which the ICCs α_{IC}^{q,nl_j} ($M1$: DS $\rightarrow 6^-$) decrease more gently with the decrease in binding energy for higher atomic shells (M, N, etc.). On the other hand, in the $E2$ NEEC process, $np_{3/2}$ orbitals play a dominant role, for which ICCs α_{IC}^{q,nl_j} ($E2$: DS $\rightarrow 6^-$) decrease more steeply for higher atomic shells.

It is worth underlining that the theoretically predicted total probability of the NEEC process for the $M1$ transition for ^{84m}Rb is also almost three orders of magnitude higher (see Table II) than the $E2$ transition for the ^{93m}Mo isomer. Inclusion of the Compton profiles of bound target electrons for capture and excited states for the capturing atom might be expected to increase these values further. As we have shown in our previous work regarding the ^{93m}Mo isomer, the excited-state configurations can provide probabilities that are a factor of about 20 higher than those obtained from the ground-state-configuration approach without Compton profiles [34]. Therefore, as a rough estimate, one can assume that taking into account both effects for ^{84m}Rb isomer may result in a similar enhancement of the $M1$ and $E2$ NEEC processes in beam-based conditions. In this work, we deliberately neglect both effects. This is related to the desire to present in the work a clear comparison of the $M1$ and $E2$ NEEC processes, not distorted by Compton profiles and excited electronic configurations effects [28,33].

V. SUMMARY AND CONCLUSIONS

The beam-based scenario for the production and depletion via NEEC of the ^{84m}Rb isomer has been considered. The NEEC process allows an excitation by $M1$ and $E2$ transitions from the 20.26-min ^{84m}Rb isomer with $I^\pi = 6^-$ to a DS with $I^\pi = 5^-$ which lies only 3.498 keV higher in energy, and has $T_{1/2} = 9$ ns. The DS decays to a 3^- state through a 219.099-keV $E2$ transition and then sequentially to the ground state, releasing a substantial amount of stored energy. The cross sections calculated by means of the PACE4 and GEMINI++ fusion-evaporation codes indicate that the ^{82}Se + ^{7}Li nuclear reaction can be used for efficient production of ^{84}Rb isotopes, especially at high beam energy (7.1–7.4 MeV/u). The necessary kinetic energies required for the NEEC process to occur have been predicted for $n = 3$, 4, 5, 6, and 7 shells of ^{84m}Rb ions in various charge states expected in subsequent stages of the ion-stopping process.

The NEEC resonance strengths and partial probabilities have been estimated in order to recognize the partial contributions to the whole NEEC process from the specific atomic orbitals. It has been found that under beam-based conditions, the resonant strengths and probabilities for the $M1$ NEEC process would dominate over $E2$ by several orders of magnitude for low-energy nuclear excitations (of the order of a few keV). The highest values of NEEC resonance strengths and probabilities one can expect are for electron captures into the $ns_{1/2}$ subshells for $M1$ and $np_{3/2}$ subshells for $E2$ nuclear excitations.

The total probability of $M1$ excitation in the ^{84m}Rb isomer was estimated at 2.13×10^{-8}. It is worth emphasizing that, to the best of our knowledge, this is the highest NEEC probability estimated theoretically for the beam-based scenario so far. This result makes the ^{84m}Rb isomer an interesting candidate for observation of the NEEC process. The total probability for $E2$ excitation of ^{84m}Rb to its DS is three orders of magnitude lower than that for $M1$ excitation. It is also worth noting that the theoretically predicted NEEC probability of the $M1$

transition for ^{84m}Rb to its DS is also three orders of magnitude higher than the $E2$ transition for the ^{93m}Mo isomer to its DS.

The authors believe that this analysis of the atomic conditions for the NEEC process should be an important step in better understanding the nature of the NEEC process in beam-based conditions.

ACKNOWLEDGMENTS

This work is supported by the National Science Centre, Poland, under Grant No. 2017/25/B/ST2/00901. This research work was supported by the Ministry of Science and Higher Education as part of the IPPLM statutory subsidy.

[1] M. Hult *et al.*, Appl. Rad. Isot. **67**, 918 (2009).
[2] I. Arnquist *et al.*, Phys. Rev. Lett. **131**, 152501 (2023).
[3] J. J. Carroll, Nuclear metastables for energy and power: Status and challenges, in *Innovations in Army Energy and Power Materials Technologies*, edited by E. C. Shaffer and T. S. Zheleva (Materials Research Forum, Millersville, PA, 2018).
[4] V. I. Goldanskii and V. A. Namiot, Phys. Lett. B **62**, 393 (1976).
[5] A. A. Zadernovsky and J. J. Carroll, Hyperfine Interact. **143**, 153 (2002).
[6] A. Pálffy, W. Scheid, and Z. Harman, Phys. Rev. A **73**, 012715 (2006).
[7] A. Pálffy, J. Evers, and C. H. Keitel, Phys. Rev. Lett. **99**, 172502 (2007).
[8] N. Cue, J.-C. Poizat, and J. Remillieux, Europhys. Lett. **8**, 19 (1989).
[9] J. J. Carroll and C. J. Chiara, Eur. Phys. J. Spec. Top. (2024).
[10] L. Bernstein, EBIT plans in Livermore and Berkeley, in *Proceedings of the ECT Workshop on Atomic Effects in Nuclear Excitation and Decay* (Trento, Italy, 2009).
[11] P. Morel, J. M. Daugas, G. Gosselin, V. Méot, and D. Gogny, AIP Conf. Proc. **769**, 1085 (2005).
[12] A. Pálffy, Z. Harman, C. Kozhuharov, C. Brandau, C. H. Keitel, W. Scheid, and T. Stöhlker, Phys. Lett. B **661**, 330 (2008).
[13] J. Gunst, Y. A. Litvinov, C. H. Keitel, and A. Pálffy, Phys. Rev. Lett. **112**, 082501 (2014).
[14] J. Gunst, Y. Wu, N. Kumar, C. H. Keitel, and A. Pálffy, Phys. Plasmas **22**, 112706 (2015).
[15] J. Gunst, Y. Wu, C. H. Keitel, and A. Pálffy, Phys. Rev. E **97**, 063205 (2018).
[16] Y. Wu, J. Gunst, C. H. Keitel, and A. Pálffy, Phys. Rev. Lett. **120**, 052504 (2018).
[17] Y. Wang, Z. Ma, Y. Yang, C. Fu, W. He, and Y. Ma, Front. Phys. **11**, 1203401 (2023).
[18] P. V. Borisyuk, N. N. Kolachevsky, A. V. Taichenachev, E. V. Tkalya, I. Y. Tolstikhina, and V. I. Yudin, Phys. Rev. C **100**, 044306 (2019).
[19] A. Y. Dzyublik, Phys. Rev. C **102**, 024604 (2020).
[20] A. Y. Dzyublik, Phys. Rev. C **106**, 064608 (2022).
[21] S. A. Karamian and J. J. Carroll, Phys. At. Nucl. **75**, 1362 (2012).
[22] M. Polasik, K. Słabkowska, J. J. Carroll, C. J. Chiara, Ł. Syrocki, E. Węder, and J. Rzadkiewicz, Phys. Rev. C **95**, 034312 (2017).
[23] C. J. Chiara, J. J. Carroll, M. P. Carpenter, J. P. Greene, D. J. Hartley, R. V. F. Janssens, G. J. Lane, J. C. Marsh, D. A. Matters, M. Polasik, J. Rzadkiewicz, D. Seweryniak, S. Zhu, S. Bottoni, A. B. Hayes, and S. A. Karamian, Nature (London) **554**, 216 (2018).
[24] J. T. Anderson *et al.*, A digital data acquisition system for the detectors at gammasphere, *IEEE Nuclear Science Symposium and Medical Imaging Conference Record (NSS/MIC) Anaheim, CA* (IEEE, Piscataway, NJ, 2012), pp. 1536–1540.
[25] Y. Wu, C. H. Keitel, and A. Pálffy, Phys. Rev. Lett. **122**, 212501 (2019).
[26] K. Słabkowska, E. Węder, Ł. Syrocki, M. Polasik, J. Rzadkiewicz, J. J. Carroll, and C. J. Chiara, Acta Phys. Pol. B **50**, 651 (2019).
[27] Ł. Syrocki, E. Węder, K. Słabkowska, M. Polasik, J. Rzadkiewicz, J. J. Carroll, and C. J. Chiara, Acta Phys. Pol. B **50**, 1359 (2019).
[28] J. Rzadkiewicz, M. Polasik, K. Słabkowska, Ł. Syrocki, E. Węder, J. J. Carroll, and C. J. Chiara, Phys. Rev. C **99**, 044309 (2019).
[29] Ł. Syrocki, K. Słabkowska, M. Polasik, E. Węder, J. Rzadkiewicz, J. J. Carroll, and C. J. Chiara, Acta Phys. Pol. B **51**, 393 (2020).
[30] S. Guo, Y. Fang, X. Zhou, and C. M. Petrache, Nature (London) **594**, E1 (2021).
[31] C. J. Chiara, J. J. Carroll, M. P. Carpenter, J. P. Greene, D. J. Hartley, R. V. F. Janssens, G. J. Lane, J. C. Marsh, D. A. Matters, M. Polasik, J. Rzadkiewicz, D. Seweryniak, S. Zhu, S. Bottoni, and A. B. Hayes, Nature (London) **594**, E3 (2021).
[32] S. Guo, B. Ding, X. H. Zhou, Y. B. Wu, J. G. Wang, S. W. Xu, Y. D. Fang, C. M. Petrache, E. A. Lawrie, Y. H. Qiang, Y. Y. Yang, H. J. Ong, J. B. Ma, J. L. Chen, F. Fang, Y. H. Yu, B. F. Lv, F. F. Zeng, Q. B. Zeng, H. Huang *et al.*, Phys. Rev. Lett. **128**, 242502 (2022).
[33] J. Rzadkiewicz, M. Polasik, K. Słabkowska, Ł. Syrocki, J. J. Carroll, and C. J. Chiara, Phys. Rev. Lett. **127**, 042501 (2021).
[34] J. Rzadkiewicz, K. Słabkowska, M. Polasik, Ł. Syrocki, J. J. Carroll, and C. J. Chiara, Phys. Rev. C **108**, L031302 (2023).
[35] D. Abriola *et al.*, Nucl. Data Sheets **110**, 2815 (2009).
[36] D. Denis-Petit, G. Gosselin, F. Hannachi, M. Tarisien, T. Bonnet, M. Comet, F. Gobet, M. Versteegen, P. Morel, V. Méot, and I. Matea, Phys. Rev. C **96**, 024604 (2017).
[37] A. Y. Dzyublik, JETP Lett. **92**, 130 (2010).
[38] O. B. Tarasov and D. Bazin, Nucl Instrum Methods Phys. Res. B **204**, 174 (2003).
[39] PACE4 fusion-evaporation reaction code, National Superconducting Cyclotron Laboratory, http://lise.nscl.msu.edu/pace4.html (2013).
[40] R. J. Charity *et al.*, Nucl. Phys. A **483**, 371 (1988).
[41] R. J. Charity, Phys. Rev. C **82**, 014610 (2010).
[42] D. Mancusi, R. J. Charity, and J. Cugnon, Phys. Rev. C **82**, 044610 (2010).
[43] A. Gavron, Phys. Rev. C **21**, 230 (1980).
[44] R. Bass, Phys. Rev. Lett. **39**, 265 (1977).
[45] C. M. Percy and F. G. Percy, At. Nucl. Data Tables **17**, 1 (1976).
[46] W. Hauser and H. Feshbach, Phys. Rev. **87**, 366 (1952).
[47] G. Schiwietz and P. L. Grande, Nucl. Instrum. Methods Phys. Res. B **175–177**, 125 (2001).
[48] I. P. Grant and H. M. Quiney, Adv. At. Mol. Phys. **23**, 37 (1988).

[49] K. G. Dyall, I. P. Grant, C. T. Johnson, F. A. Parpia, and E. P. Plummer, Comput. Phys. Commun. **55**, 425 (1989).
[50] M. Polasik, Phys. Rev. A **39**, 616 (1989).
[51] M. Polasik, K. Słabkowska, J. Rzadkiewicz, K. Kozioł, J. Starosta, E. Wiatrowska-Kozioł, J. C. Dousse, and J. Hoszowska, Phys. Rev. Lett. **107**, 073001 (2011).
[52] M. R. Harston and J. F. Chemin, Phys. Rev. C **59**, 2462 (1999).
[53] M. Honma, T. Otsuka, T. Mizusaki, and M. Hjorth-Jensen, Phys. Rev. C **80**, 064323 (2009).
[54] P. Ring and P. Schuck, *The Nuclear Many-Body Problem* (Springer-Verlag, New York, 1980).
[55] S. Raman, C. W. Nestor Jr., A. Ichihara, and M. B. Trzhaskovskaya, Phys. Rev. C **66**, 044312 (2002).
[56] T. Kibédi, T. W. Burrows, M. B. Trzhaskovskaya, P. M. Davidson, and C. W. Nestor, Jr., Nucl. Instrum. Methods Phys. Res. A **589**, 202 (2008).
[57] S. Gargiulo, I. Madan, and F. Carbone, Phys. Rev. Lett. **128**, 212502 (2022).